Construction and Building Materials 327 (2022) 126983

Contents lists available at ScienceDirect

Construction and Building Materials

journal homepage: www.elsevier.com/locate/conbuildmat

Weathered bottom ash from municipal solid waste incineration: Alkaline activation for sustainable binders

A. Maldonado-Alameda [a,*], Jessica Giro-Paloma [a], Fernanda Andreola [b], Luisa Barbieri [b], J. M. Chimenos [a], Isabella Lancellotti [b]

[a] Departament de Ciència de Materials i Química Física, Universitat de Barcelona, C/ Martí i Franquès, 1-11, 08028, Barcelona, Spain
[b] Department of Engineering "Enzo Ferrari", Università degli Studi di Modena e Reggio Emilia, Via Pietro Vivarelli 10, 41125, Modena, Italy

ARTICLE INFO

Keywords:
Weathered bottom ash
Metakaolin
Alkali-activated binders
Waste management
Municipal solid waste incineration

ABSTRACT

Alkali-activated binders (AABs) stand out as promising candidates to replace ordinary Portland cement (OPC) since waste can be used as raw material for their manufacture. This study addresses the environmental feasibility of using weathered bottom ash (WBA) and metakaolin (MK) as alkali-activated binder precursors (AA-WBA/MK). Different proportions of WBA and MK were mixed (100/0, 75/25, 50/50, 25/75, and 0/100 wt%) with a mixture of waterglass (WG) and NaOH 8 M as an alkaline activator solution. The effect of increasing MK content was assessed from a chemical, physical, mechanical, and environmental perspective. The results revealed the formation of secondary reaction products of C-(A)-S-H, (C,N)-A-S-H, and N-A-S-H gels. The compressive strength of AA-WBA/MK binders decreased (from 61.6 MPa to 12.6 MPa) as the MK content increased. The monolithic tank test validated the use of AA-WBA/MK binders for construction purposes, although with some restrictions due to their content in As, Sb, and V. Finally, the encapsulation efficiency and mechanical performance of AA-WBA/MK binders was enhanced as the curing period increased.

1. Introduction

Waste management (WM) has become one of the main concerns of the European Union (EU) in recent decades [1]. The main challenge is to achieve suitable management based on waste prevention, reuse and recycling, which leads to a more environmentally friendly economy [2,3]. Many countries choose waste-to-energy (WtE) as the main alternative to avoid the environmental issues generated by municipal solid waste (MSW) landfilling [4–7]. In 2019, 224 Mt of MSW were produced in the EU, 26% of which was incinerated in WtE plants [8]. In MSW incineration (MSWI), energy is recovered from unsorted waste fractions. This process reduces the waste volume by 90% and the waste weight by 75% [9,10]. Three countries (Germany, France and Italy) are responsible for 60% of the total amount of waste incinerated in the EU. In Spain, MSWI has increased by around 25% in the last 10 years, reaching 2.5 Mt in 2019 [8]. The solution of recovering energy in WtE plants in Spain is a good alternative considering that 54% of MSW ended up in landfill in 2019 [8].

Incinerated bottom ash (IBA) is the main by-product of MSWI. It accounts for 85% of the solid resulting from combustion [11]. IBA is classified as hazardous or non-hazardous waste by the European waste catalogue (EWC), depending on its concentration of hazardous compounds [12]. IBA needs a natural weathering treatment for its valorisation as a secondary material. This consists of storing it outdoors in stockpiles for 2 to 3 months to obtain an unbound granular material known as weathered bottom ash (WBA) [13]. This treatment leads to chemical stabilisation and a reduction in the solubility and mobility of toxic elements through carbonation, oxidation, precipitation and pH neutralisation reactions [14]. The final composition of WBA (rich in SiO_2, CaO and Al_2O_3) means that it can be applied in building, civil engineering [15–19], and chemical engineering [20,21] fields. However, some chemical, legal and technological barriers linked to potential leaching toxicity hamper its valorisation in many countries due to the heavy metal(loid)s contained in WBA [12,22,23]. For this reason, alkali activation of WBA stands out as a suitable option to achieve heavy metal (loid) stabilisation in a cementitious matrix.

Alkali activation consists of the reaction between an aluminosilicate-rich precursor powder and an alkaline activator solution to obtain a compact cementitious matrix [24]. There are environmental reasons supporting the use of alkali-activated cements (AACs) instead of

* Corresponding author.
E-mail address: alex.maldonado@ub.edu (A. Maldonado-Alameda).

https://doi.org/10.1016/j.conbuildmat.2022.126983
Received 29 July 2021; Received in revised form 24 January 2022; Accepted 23 February 2022
Available online 2 March 2022
0950-0618/© 2022 The Author(s). Published by Elsevier Ltd. This is an open access article under the CC BY-NC-ND license (http://creativecommons.org/licenses/by-nc-nd/4.0/).

Table 1
Alkali-activated binders' formulations by WBA/MK mixture.

Reference	S [1]WBA (wt.%)	[1]MK(wt. %)	L [1]NaOH(wt. %)	[1]Na_2SiO_3(wt. %)	L/S ratio	SiO_2/Al_2O_3	Na_2O/Al_2O_3	[2]SiO_2/Na_2O	Alkali-activator solution pH
100 W	100	0	1612345266	64	0.8	19.4	4.4	2.1	12.7
75W25M	75	25		47	0.6	6.1	0.9	2.0	12.9
50W50M	50	50		47	0.8	4.2	0.9	1.2	>14.0
25W75M	25	75		52	1.0	3.5	0.9	1.1	>14.0
100 M	0	100		68	1.3	3.0	0.9	1.0	>14.0

[1] *wt% respect to the total solid*
[2] *Ms of alkali-activator solution (molar ratio)*

ordinary Portland cement (OPC). AACs offer innovative and ingenious solutions to reduce energy consumption and greenhouse gas (GHG) emissions associated with the manufacture of OPC [25–27]. Besides, most AAC precursors are industrial by-products or waste, which favours the zero-waste principle and the circular economy promoted by new EU policies [3,28]. However, the hazardousness of AACs can be enhanced substantially by the combination of these precursors with highly alkaline media. During the service life of AACs, toxic elements such as trace metals, polycyclic aromatic hydrocarbons (PAH), dissolved organic carbon (DOC), sulphates, chlorides and fluorides could be released into the environment [29,30]. Therefore, it is important to assess environmental viability through tests that allow the potential toxicity and environmental behaviour of these cement-based materials to be determined [31]. The requirements of AACs must not only be related to their properties or the safety of buildings but also to the health and protection of the environment, as stated in Regulation No 305/2011 of the European Parliament.

Many studies in the last decade have evidenced the possibilities of using alkali activation of WBA to formulate AACs [32–37]. WBA has been mixed with a wide range of materials for use as precursors. These include natural raw materials such as metakaolin (MK) [38–42] and slaked lime (SL) [43], industrial by-products such as fly ash (FA) [44] and granulated blast furnace slag (GBFS) [37,45] or urban wastes such as incineration fly ash (IFA) [46,47] and drinking water treatment residue (DWTR) [48]. The microstructure, chemical stability and mechanical properties of alkali-activated WBA (AA-WBA) binders and mortars have been exhaustively studied in the literature [49]. Nonetheless, the environmental risk assessment of these materials should be further investigated, due to the heavy metal(loid)s contained in WBA [23]. Some studies have evaluated the leaching concentration of metal (loid)s through granular (EN 12457–2 [32] and 12457–4 [47,50]) and monolithic (TCLP [46,48,51], ANSI/ANS [46], and NEN 7375 [52]) leaching tests. However, most of the studies did not analyse the leaching concentration of arsenic (only in some cases) and antimony, whose significant presence in AA-WBA binders' leachates has been demonstrated by the authors elsewhere [31,53–56]. Indeed, the leaching concentration of both metal(loid)s in AA-WBA binders was above the non-hazardous waste limit set by European landfill legislation [57]. Hence, it is extremely important to analyse all heavy metal(loid)s to ensure that their use as building material does not have any environmental impact and complies with the requirements set by European standards for construction materials.

The present research is focused on the formulation of new alkali-activated binders (AABs) using WBA and MK (AA-WBA/MK), to contribute to the development of more sustainable construction cements. The main goal of this study was to assess the effect of adding different percentages of MK on the final properties of AA-WBA/MK binders. The originality of this research is based on an exhaustive assessment of environmental properties through granular (EN 12457–2) and monolithic (CEN/TS 16637–2) leaching tests to simulate the service life scenario and end-of-life scenario of AA-WBA/MK binders, and the use of the 8 to 30 mm fraction and MK to enhance mechanical and environmental properties. This WBA fraction has the highest SiO_2 availability in the WBA [53], while the metallic aluminium (Al) contained is lower than WBA fine fractions due to the recovery effectiveness of the Eddy current device for particles above 6 mm [11]. Both can lead to a decrease in porosity generated by the reaction of Al and NaOH and contribute to enhancing the mechanical behaviour of AA-WBA/MK binders. The use of the 8 to 30 mm fraction can increase environmental feasibility and reduce the heavy metal(loid)s content, as already demonstrated [13,53]. In addition, the use of MK can balance the lack of reactive aluminium in WBA, enhance strength development and the AAC polycondensation reaction [58,59]. Its chemical composition is less polluting than WBA, which can contribute to improving the environmental properties through the dilution of heavy metal(loid)s in the binder matrix that is obtained. The properties of AA-WBA/MK formulations were determined from a physicochemical, physical, mechanical, and environmental perspective. Special attention was paid to environmental characterisation, since this study aimed to develop sustainable binders, promote the zero-waste principle, and contribute to the search for a greener alternative to OPC pastes.

2. Experimental procedure

2.1. Materials

WBA was supplied and collected at the VECSA facilities, the company that conditions and revalorises the bottom ash generated at the WtE plant in Tarragona (Spain). Commercial Metakaolin (MK) powder was supplied by Bal-Co (Italy). A mixture of sodium silicate (Na_2SiO_3) and sodium hydroxide (NaOH) was used as the alkaline activator solution. The Na_2SiO_3 solution with molar ratio $SiO_2/Na_2O = 3.22$ (26.44% of SiO_2 and 8.21% of Na_2O; $\rho = 1.37\ g{\cdot}cm^{-3}$) was supplied by Scharlab, S. L. and the 8 M NaOH solution ($\rho = 1.24\ g{\cdot}cm^{-3}$) was prepared using pellets (Labbox Labware S.L.; purity > 98%) and deionised water.

2.2. WBA preparation

The 60 kg WBA sample that was collected was quartered to obtain a representative sample of 15 kg. Then, the sample was dried on a stove at 105 °C for 24 h and sieved to obtain the 8 to 30 mm fraction (30% of the total mass). Afterwards, the remaining magnetic particles in WBA (6.57% of the total mass) were removed by a magnet (Nd; 0.485 T) before crushing and milling with a jaw crusher RETSCH BB 50 and a vibratory disc mill RETSCH RS20, respectively. A powder with a particle size of<80 μm was obtained to favour reactivity and homogeneity between the two precursors, since the particle size of MK powder was 75 μm.

2.3. Raw materials characterization

X-ray fluorescence (XRF) elemental analysis of WBA was conducted by a spectrophotometer Panalytical Philips PW 2400 sequential X-ray equipped with the software UniQuant® V5.0. Mineralogical analysis of MK and WBA was carried out using a Bragg-Brentano Siemens D-500 powder diffractometer device with CuKα radiation to determine the

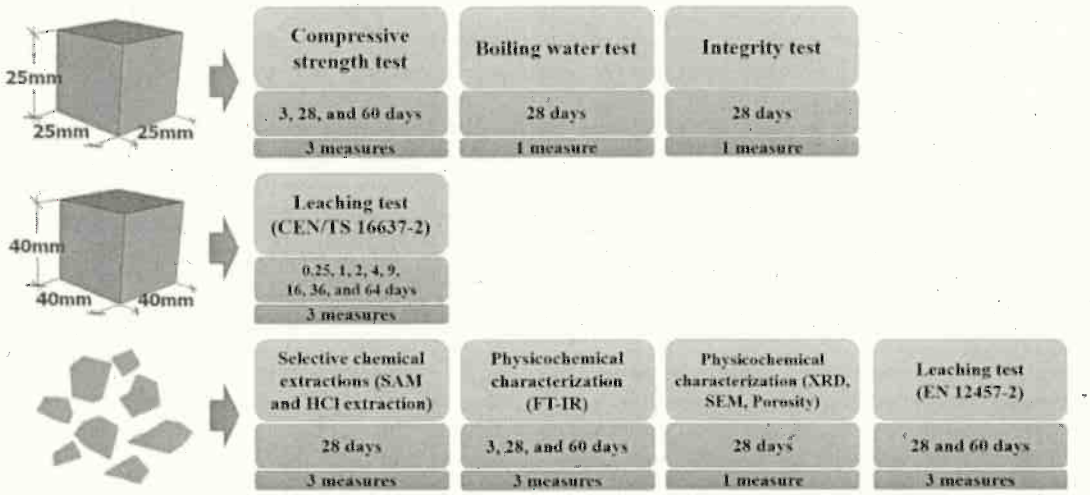

Fig. 1. Tests scheme.

crystalline phases of WBA. The SiO_2/Al_2O_3 availability of WBA and MK was determined by chemical attack with NaOH solution to determine the reactive phase of precursors [60]. One gram of powder raw materials was placed in a 100 mL 8 M NaOH solution and stirred constantly for 5 h in a sealed Teflon beaker at 80 °C. The resulting solution was filtered and analysed by Perkin Elmer Optima ICP-OES 3200 RL equipment to quantify the Si and Al content. Leaching tests were conducted using European standard EN 12457–2 to evaluate the hazardousness of WBA according to the acceptance limits for landfills established by the EU [57]. The leachate analysis was carried out by means of an ICP-MS Perkin-Elmer Elan-6000 device.

2.4. Samples preparation

Five formulations with different MK/WBA content (Table 1) were prepared to assess the effect of increasing the WBA content on the final structure and properties of AA-WBA/MK binders. The workability of pastes was determined by the mini-slump test procedure reported in the literature [61]. The spread diameters were in the range of 105 to 120 mm. The Na_2O/Al_2O_3 ratio by wt. % was adjusted to 0.9 considering the Si, Al, and Na weight percentages from the precursors (WBA and MK) and activators (Na_2SiO_3 and NaOH solutions). The value of the Na_2O/Al_2O_3 ratio leads to an improvement in the dissolution step of Si^{4+} and Al^{3+} and enhances the polymerization process [62]. The SiO_2/Al_2O_3 ratio could not be adjusted as the higher the WBA content, the higher the SiO_2/Al_2O_3 ratio. This is because of the lack of reactive aluminium in the WBA precursor. In the case of the 100 W formulation, both ratios could not be adjusted, and the authors used the formulation reported elsewhere [55].

The preparation of the formulations consisted of the following steps:

(i) Weighing and mixing in a plastic beaker the WBA/MK powder and the activating solutions, separately, to homogenize both mixtures.

(ii) Gradually adding the activating solutions to the powder mixture of WBA/MK and stirring mechanically for 5 min at 760 rpm, to favour precursor dissolution and to obtain a homogeneous and fluid paste.

(iii) Pouring the paste into silicon cubic-shape moulds (25x25x25 mm and 40x40x40 mm) and putting these in a plastic sealed bag at room temperature for three days to avoid loss of water (setting and initial curing phase).

(iv) Removing the moulds from the plastic sealed bag and unmoulding the specimens, keeping them at room temperature and humidity (25 °C ± 1 °C and relative humidity of 50% ± 5%) until the day of the tests (curing phase).

2.5. Hydrolytic stability tests

All formulations were subjected to an integrity test, which consisted of immersing one specimen of each formulation in deionised water for 48 h [39]. The specimens were also exposed to boiling water tests based on placing them into the water at 100 °C for 20 min [54]. In both cases, the specimens were tested after 28 days of curing and dried in a desiccator with silica gel until constant weight. The weight loss percentages were calculated after the two tests. These tests allow the hydrolytic stability to be evaluated and therefore the formation of binder phases and their cohesion with the non-reacting mineral phases during the alkali activation process.

2.6. Alkali-activated binders' characterisation

The AA-WBA/MK characterisation was determined through various characterisation methods and tests. Some of them were carried out at different ages (3, 28 and 60 days) to fully understand the alkali activation process (Fig. 1).

Salicylic acid/methanol (SAM) and hydrochloric acid (HCl) dissolution treatments were conducted to evaluate the formation of C-(A)-S-H and N-A-S-H phases [63]. SAM and HCl extraction were performed by attacking 1 g of powdered AABs in a salicylic acid/methanol solution for 1 h (5 g of salicylic acid and 40 mL of methanol) and 250 mL solution of HCl (1:20 by volume) for 3 h, respectively. Then, the solutions were filtered (Whatman filter, 20 μm pore size). The residual fraction (RF) was washed and dried in a desiccator with silica gel until constant weight to calculate the mass that was dissolved. The mass dissolved by SAM solution indicated the presence of C-(A)-S-H phases while the mass dissolved by HCl solution revealed the presence of C-(A)-S-H, N-A-S-H and carbonate phases [64].

X-ray diffraction (XRD) analysis was performed to determine the new crystalline phases and main reaction products in AA-WBA/MK, using a Bragg-Brentano Siemens D-500 powder diffractometer device with CuKα radiation.

Fourier transformed infrared spectroscopy (FT-IR) in attenuated total reflectance mode (ATR) was carried out to evaluate the new formation, changing and rupture of bonds by comparing the initial precursors' powders and AA-WBA/MK binders. A 32-scan average with 4 cm^{-1} resolution (in the 4000 to 400 cm^{-1} range) was collected by Spectrum Two™ equipment from Perkin Elmer. The range (1200–800 cm^{-1}) ascribed to the C-(A)-S-H phases was deconvoluted using Gaussian functions with computer software, following the criteria reported elsewhere [65].

The microstructure observation was conducted by scanning electron

Table 2
Chemical composition of raw materials.

Element(wt. %)	SiO_2	Al_2O_3	Na_2O	K_2O	Fe_2O_3	CaO	MgO	TiO_2	LOI
[1]MK	55.0	40.0	[2]0.8		1.4	[2]0.3		1.5	1.0
WBA	52.08	6.35	3.38	2.09	4.12	20.72	2.43	0.65	6.1

[1] Chemical analysis indicated on the product technical datasheet.
[2] Sum of Na_2O and K_2O, and CaO and MgO, respectively.

microscopy-energy dispersive spectroscopy (SEM-EDS) ESEM FEI Quanta 200 equipment. The energy-dispersive X-ray spectroscopy (EDS) analysis was also performed to determine the SiO_2/Al_2O_3 and Al_2O_3/Na_2O ratios. Fractured specimens of the samples after the compressive strength test were used. The samples were impregnated with epoxy, polished with SiC papers, and coated with graphite. The micrographs were collected at voltages of 20 kV and a working distance of around 10 mm.

The bulk density (ρ_a) and porosity (Φ) after 28 curing days were determined to better understand the mechanical behaviour of AA-WBA/MK binders. The porous network of each formulation was analysed with the mercury (Hg) intrusion porosimetry (MIP) technique using porosimeter Micromeritics Autopore IV 9510 equipment. Hg intrusion porosimetry was carried out to measure pore size distributions, total pore volume, total pore surface area and bulk density. Fractured specimens after the compressive strength tests (σ_c) were dried in a stove at 50 °C to remove humidity before the mercury intrusion [66]. Then, about 1 g of dried samples was put in a penetrometer with a 15 mL sample cup and steam volume of 0.38 mL. The operative conditions were fixed to identify capillary pores between 0.006 and 350 μm at (i) equilibrium time (10 sec) and (ii) pressure limits of 345 kPa and 228 MPa permits.

The compressive strength (σ_c) tests after 3, 28 and 60 curing days were performed by Incotecnic MULTI-R1 equipment (loading rate of 240 $kg{\cdot}s^{-1}$ until fracture). Three measures per formulation were conducted.

Leaching tests were performed to evaluate the potential metal(loid) release of the AA-WBA/MK. During the alkali activation process, some pH-dependent heavy metal(loid)s could be mobilised due to the alkaline activator solution's high pH [54]. The heavy metal(loid) leaching concentrations of each formulation were analysed following European standards EN 12457–2 and CEN/TS 16637–2. The former was used to simulate leaching behaviour after potential demolition (end-of-life scenario). The second was conducted to assess the leaching potential of the samples under service life conditions (service life scenario). The powdered raw materials and crushed fragments (particles below 4 mm) of AA-WBA/MK binders obtained after the compressive strength test were used to perform the granular leaching test (EN 12457–2). The fragments were in continuous rotating agitation (10 min^{-1}) with deionised water (L/S ratio of 10 $L{\cdot}kg^{-1}$) for 24 h at room temperature. Monolithic specimens (40-mm cubic size) were used to follow the CEN/TS 16637–2 standard. The specimens were submerged in deionised water (water volume to surface area was 80 ± 10 $L{\cdot}m^{-2}$) at room temperature. The solvent was exchanged at cumulative time intervals of 0.25, 1, 2.25, 4, 9, 16, 36 and 64 days. The eluate of each interval and formulation was then sampled. The resulting leachates in both leaching tests were filtered with a 0.45-μm nitrocellulose membrane. Two replicas per sample and one aliquot per replica were analysed by the inductively coupled plasma mass spectrometry (ICP-MS) technique with a PerkinElmer ELAN device. The concentrations of As, Ba, Cd, Cr, Cu, Hg, Mo, Ni, Pb, Sb, Se, V and Zn were evaluated. The results of the granular test (EN 12457–2) were compared with the landfill acceptance limits established by EU legislation [57], to determine the hazardousness of AA-WBA/MK binders. Concerning the monolithic test (CEN/TS 16637–2), the cumulative metal(loid) release ($mg{\cdot}m^{-2}$) of AA-WBA/MK binders was compared to the limits established in the Dutch Building Materials Decree. This standard allows construction materials to be classified into two categories [67]: (i) materials below the U_1 limit, with no environmental restriction and (ii) materials that exceed the U_2 limit, which should be used with restrictions and dismantled at their end of life. For materials whose cumulative metal(loid) release is between the U_1 and U_2 limits, the pollutant that exceeds the threshold should be removed at the end of their lifecycle [68].

3. Results and discussion

3.1. Raw materials characterization

The major oxide elements of WBA and MK are given in Table 2. As shown, both precursors are rich in SiO_2, CaO and Al_2O_3, which are key elements to obtain AABs.

The mineralogical analysis of WBA (Fig. 2a) confirms that the identified phases are mainly constituted of Si, Al, and Ca compounds. Quartz (SiO_2; PDF# 01–079-1910) and calcite ($CaCO_3$; PDF# 01–083-1762) were detected as the main crystalline phases. Dolomite ($CaMg(CO_3)_2$; PDF# 01–075-1759), akermanite ($Ca_2Mg(Si_2O_7)$; PDF# 01–079-

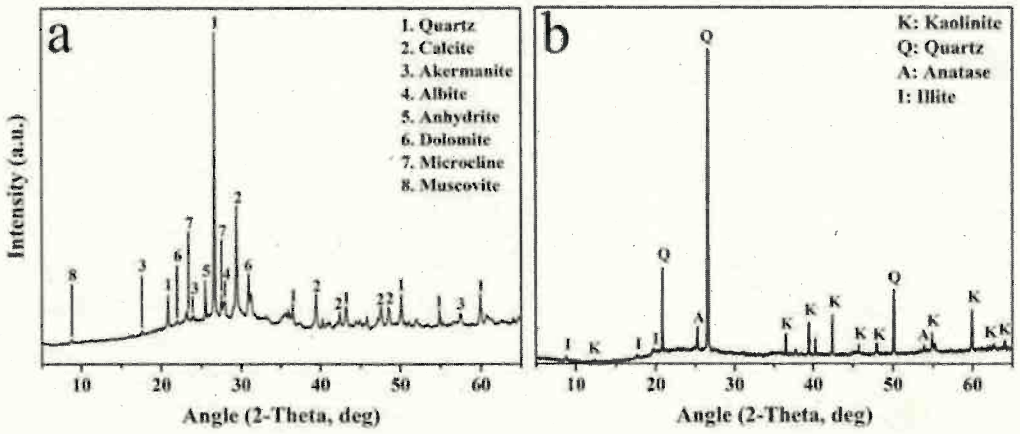

Fig. 2. XRD patterns of (a) WBA (b) MK.

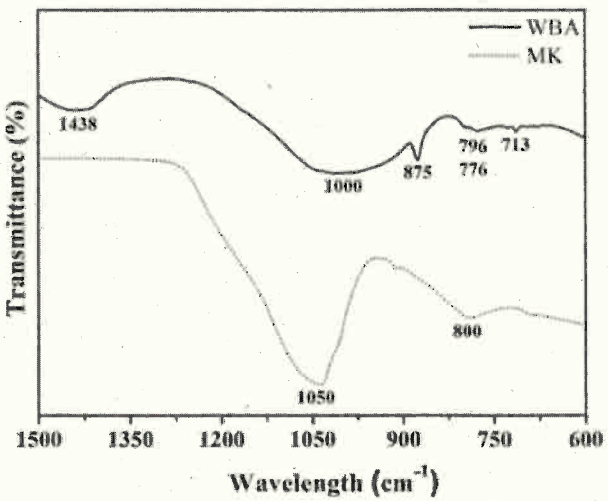

Fig. 3. Raw materials FT-IR spectra.

Table 3
SiO_2 and Al_2O_3 availability of MK and WBA.

	SiO_2 (wt. %)	Reactive %	Al_2O_3 (wt. %)	Reactive %
MK	46.01	84	36.46	91
WBA	21.66	42	2.89	45

2424), anhydrite ($CaSO_4$; PDF# 01–072-0503), albite calcian ordered ($(Na,Ca)Al(Si,Al)_3O_8$); PDF# 020–0548), microcline ($KAlSi_3O_8$; PDF# 01–076-0918) and muscovite ($KAl_2(AlSi_3O_{10})(OH)_2$; PDF# 01–077-2255) were also detected. The sample was of a partially vitreous nature due to the presence of a halo between 20° and 35°. The XRD pattern of MK (Fig. 2b) reveals the presence of Quartz (SiO_2; PDF# 01–078-2315) and Kaolinite ($Al_2Si_2O_5(OH)_4$; PDF# 01–075-1593) as the main phases, as well as traces of Anatase (TiO_2; PDF# 01–078-2486) and Illite ($(K,H_3O)(AlMgFe)_2(Si,Al)_4O_{10}$; PDF# 026–0911).

FT-IR spectra of MK and WBA (Fig. 3) show two broad bands (at 1050 cm^{-1} and 1000 cm^{-1}, respectively) attributed to the asymmetric T–O (T = Si or Al) stretching mode. The broad shoulder of the MK spectrum at 800 cm^{-1} is ascribed to the symmetric Al-O stretching vibration. Three peaks related to the stretching (1436 cm^{-1}) and bending modes (875 cm^{-1} and 713 cm^{-1}) of the WBA carbonates phases were also observed, and two peaks at 796 cm^{-1} and 776 cm^{-1} corresponding to quartz. These results agree with the phases identified in the XRD.

Table 3 summarises the reactive phase's availability in raw materials, determined by a chemical attack in NaOH 8 M solution. Compared with the XRF analysis shown in Table 2, the results revealed that most of the SiO_2 and Al_2O_3 content in MK is reactive. However, SiO_2 and Al_2O_3 availability is substantially reduced in the WBA due to the large amount of natural and synthetic ceramics contained in this raw material [11]. Therefore, as expected by the authors, MK is an aluminosilicate-rich source while WBA is a silica-rich source with a substantial lack of aluminium.

Table 4 shows the leaching concentration of heavy metal(loid)s found in the eluates after the leaching test according to the EN 12457–2 standard, and the thresholds established by the EU for waste acceptance at landfills. Accordingly, WBA and MK should be classified as non-hazardous materials since the leaching concentration of Sb (in the WBA) and Ni and Se (in the MK) exceed the limits for inert waste material [57]. Therefore, from the environmental perspective, the starting raw materials (WBA and MK) can be considered suitable as secondary materials used as precursors in the formulation of AACs.

3.2. Chemical stability tests

A qualitative evaluation of the integrity test and boiling water test showed that all the monolithic samples (see Fig. 1) remained unaltered after contact with deionised water The weight loss percentage in the boiling test was 2.75% (100 W), 2.92% (75W25M), 1.71% (50W50M), 3.03% (25W75M) and 2.37% (100 M). The results in the integrity test were lower because the test was less aggressive: 1.64% (100 W), 1.07% (75W25M), 0.53% (50W50M), 1.14% (25W75M) and 1.17% (100 M). Both tests evidenced the resistance of AA-WBA/MK binders to dissolution in deionised water and the structural cohesion of all monolithic samples and formulations. This indicates the binder phases were mainly due to the alkali activation of the precursors (WBA and MK) and not to the drying of water glass (Na_2SiO_3) used as an activator.

3.3. AA-WBA/MK binders' characterisation

3.3.1. Selective chemical extractions

Fig. 4 shows the mass dissolved percentages (wt. %) of WBA, MK and AA-WBA/MK binders after SAM and HCl extraction. In the SAM extraction results, only a small amount of C-(A)-S-H was dissolved in WBA (4.5%) and MK (2.2%). This is because of the very low presence of calcium in MK, as shown in the XRF and XRD characterisation, while in the WBA (size fraction > 8 mm) the calcium is mainly found in synthetic

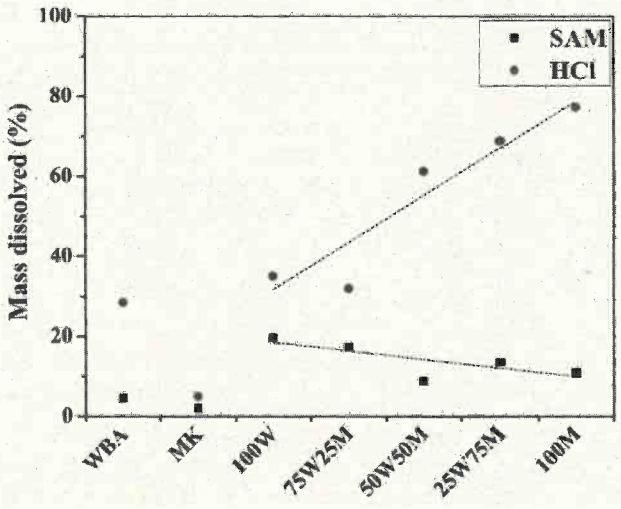

Fig. 4. Mass dissolved percentage after selective chemical extractions.

Table 4
Leaching concentrations (mg·kg^{-1}) on WBA after leaching test (EN 12457–2) and limits for acceptance at landfills.

Sample	As	Ba	Cd	Cr	Cu	Hg	Mo	Ni	Pb	Sb	Se	Zn
WBA	0.02	0.25	<0.01	0.17	0.69	0.01	0.33	0.11	0.01	0.27	<0.01	0.12
MK	0.01	0.84	<0.01	0.04	0.02	<0.01	0.01	0.53	<0.01	0.01	0.20	0.18
[1]Inert waste (mg·kg^{-1})	0.5	20	0.04	0.5	2	0.01	0.5	0.4	0.5	0.06	0.1	4
[1]Non-hazardous waste (mg·kg^{-1})	2	100	1	10	50	0.2	10	10	10	0.7	0.5	50
[1]Hazardous waste (mg·kg^{-1})	25	300	5	70	100	2	30	40	50	5	7	200

[1] limit for acceptance at landfills[57]

Table 5
Crystalline phases in AA-WBA/MK binders.

Identified phase	PDF	100 W	75W25MK	50W50MK	25W75MK	100 M
Albite ($NaAlSi_3O_8$)	01–083-1609				✓	✓
Albite calcian low ($Na_{0.84}Ca_{0.16}Al_{1.16}Si_{2.84}O_8$)	01–076-0927	✓	✓	✓		
Anhortite ($CaAl_2Si_2O_8$)	00–041-1486				✓	
Anorthoclase ($Na_{0.75}K_{0.25})(AlSi_3O_8$)	01–075-1633			✓		
Calcite ($CaCO_3$)	01–072-1937	✓	✓	✓	✓	
Calcium Silicate Hydrate ($Ca_6Si_3O_{12}H_2O$)	011–0507	✓	✓	✓	✓	
Dehydroxilated muscovite ($KAl_3Si_3O_{11}$)	046–0741					✓
Dehydroxilated paragonite ($NaAl_3Si_3O_{11}$)	046–0740					✓
Gehlenite($Ca(Al(AlSi)O_7$)	01–073-2041	✓				
Nepheline ($Na_3K(Si_{0.56}Al_{0.44})_8O_{16}$)	01–076-2468					✓
Tokkoite ($K_{1.6}Ca_{3.94}(Si_7O_{18}(OH)(OH)$)	01–079-1981	✓	✓			
Quartz (SiO_2)	01–078-2315	✓	✓	✓	✓	✓
Natron ($Na_2CO_310H_2O$)	01–082-1811		✓	✓	✓	

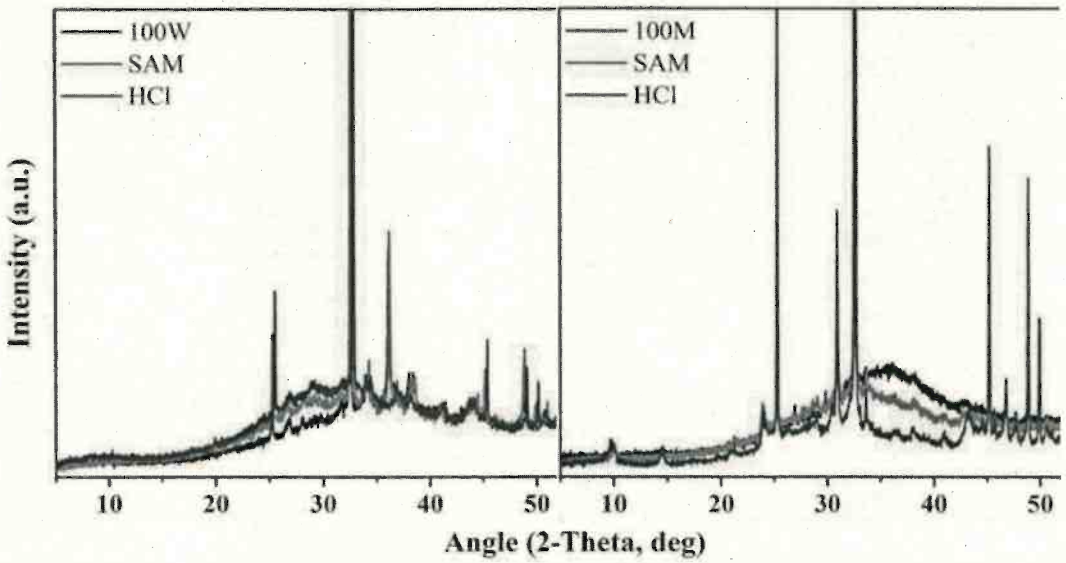

Fig. 5. XRD patterns of 100 W and 100 M before and after SAM/HCl extractions.

fired ceramics and in some carbonate (calcite) or sulphate (anhydrite) mineral phases, which are not dissolved by the SAM attack. Around 30% of the weight was dissolved by HCl extraction in the WBA mainly due to the high presence of carbonate phases such as calcite [69] and metal (hydr)oxides. In the case of MK, the mass dissolved by HCl extraction was 5.1% due to mild chemical activation of amorphous phases under acid conditions [70].

The results for the AA-WBA/MK binders reveal the formation of C-(A)-S-H and N-A-S-H phases. As expected, in the HCl extraction the percentage of dissolved mass increased as the amount of MK increased. This was due to the higher alkaline activation and formation of N-A-S-H gels when higher percentages of dehydroxylated clay were used. Along with the N-A-S-H phases, the (N, C)-(A)-S-H phases from the alkaline activation of WBA, and the calcite and other basic mineral phases contained in this precursor, were also dissolved. Likewise, a decrease in the dissolved mass was observed in the extraction of SAM as the amount of MK increased, due to the lower presence of C-(A)-S-H phases from the alkaline activation of WBA. However, in SAM extraction, the dissolved mass for 100 M (100% MK) was 11%, when the values were close to zero, due to the absence of C-(A)-S-H phases [71]. Alternatively, it should be equal to the dissolved mass of the inactivated MK (around 2–3%). This could be justified by the unexpected dissolution of a higher amount of the dry water glass (Na_2SiO_3) used as activator. When granular material was used in the SAM extraction test (see Fig. 1), the specific surface area was greater than in the monolithic test (integrity test), which increased the dissolution of these inconsistent phases. This indicates that the SiO_2/Al_2O_3 ratio was greater than that necessary for the formation of only N-(A)-S-H gels.

3.3.2. Physicochemical characterisation

3.3.2.1. X-ray diffraction (XRD) analysis. Table 5 shows the main crystalline phases found in the AA-WBA/MK binders. Quartz and calcite were identified in all formulations (except in the 100 M formulation). These phases were found in raw materials, remain unreacted in the cement matrix, and probably act as filler. Calcium silicate hydrate (C-S-H) as the main reaction product and tokkoite, gehlenite and anorthite as secondary reaction products attributed to the C-(A)-S-H phases were identified in formulations containing WBA. Albite phases, which are ascribed to the N-A-S-H and (C,N)-A-S-H phases, were also observed. The other three reaction products associated with the N-A-S-H and K-A-S-H gel such as nepheline, dehydroxylate paragonite and dehydroxylate muscovite were detected in the 100 M formulation. Finally, a sodium carbonate phase (natron), which was probably formed due to the carbonation of unreacted Na_2O, was identified in formulations activated with a mixture of two precursors.

Fig. 5 shows XRD patterns of the 100 W and 100 M samples and their respective SAM and HCl residual fractions (RFs). In both samples, significant changes in the shape and position of the amorphous hump can be observed. In addition, some peaks related to the secondary reaction products of C-(A)-S-H and N-A-S-H gels disappeared. The SAM and HCl

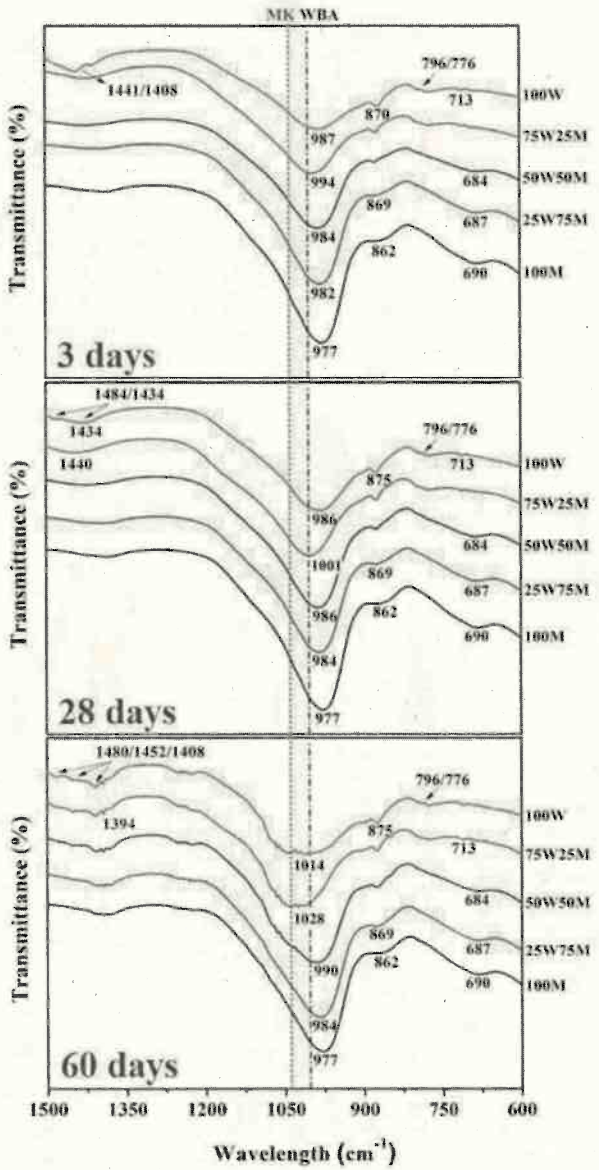

Fig. 6. AA-WBA/MK binders FT-IR spectra at 3d, 28d, and 60d.

RFs of the 100 W sample showed a substantial change in position (shift to a lower angle) and shape of the amorphous hump, which indicated the variation in composition of amorphous phases. Other investigations of alkali-activated IBA [63,72] had previously detected this variation in the amorphous hump. In addition, the RF after SAM extraction evidenced the dissolution of C-(A)-S-H phases such as gehlenite and tokkoite. The RF after HCl extraction also demonstrated the dissolution of carbonate (calcite) and aluminosilicate (albite) phases. Indeed, the only crystalline phase present after HCl extraction was quartz. As for the 100 M sample, a significant reduction of the amorphous hump in both SAM and HCl extractions could be identified. The RF of SAM extraction revealed the presence of crystalline phases that were typical from TiO_2, such as anatase (PDF# 01–078-2486) and rutile (PDF# 01–072-1148). These phases were indiscernible before the chemical attack. Another secondary product associated with N-A-S-H gels, such as muscovite ($KAl_2Si_3AlO_{10}(OH)_2$; PDF# 00–007-0032), was detected. The reduction of the amorphous hump was more pronounced in the RF of HCl extraction, which reveals the N-A-S-H nature of the gel formed in the 100 M sample. In this case, the crystalline phases that remained unaltered after the chemical attack were quartz, rutile, anatase, and kaolinite ($Al_2(Si_2O_5)(OH)_4$; PDF# 01–080-0886). Therefore, the XRD analysis was consistent

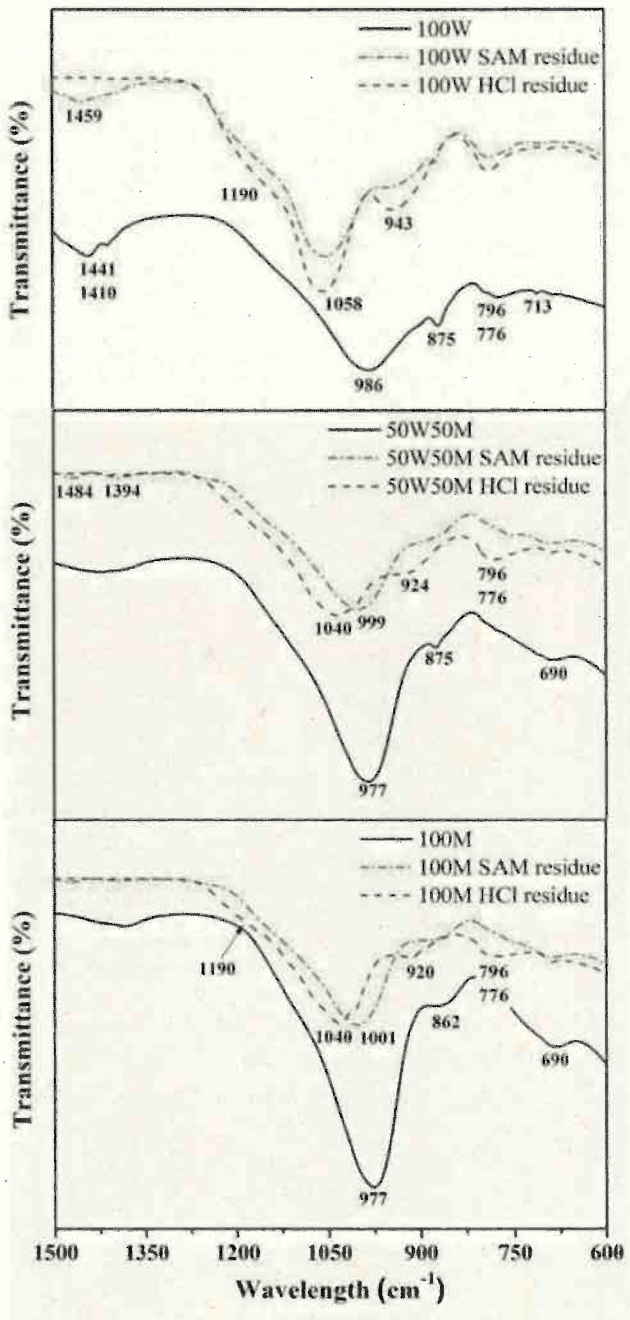

Fig. 7. AA-WBA/MK binders FT-IR spectra before and after SAM/HCl extractions.

with the selective chemical extractions results shown in section 3.3.1.

3.3.2.2. Fourier transform infrared (FT-IR) analysis. Fig. 6 depicts the FT-IR spectra of AA-WBA/MK binders at different curing times (3d, 28d and 60d). The lines indicate the position of the broadband assigned to the asymmetric T–O (T = Si or Al) stretching mode of the MK (short red dash) and the WBA (black dash and dot). The shaping changes (mainly sharpening) and shifting of the broad bands in all formulations reveal the alkali activation of raw materials and the formation of new phases [64,73]. In the samples with high-MK content (100 M, 25W75M and 50W50M), the disappearance of the MK band at 800 cm^{-1} (ν_s Al-O) and the appearance of a new band at ≈700 cm^{-1} also evidences the formation of the N-A-S-H gel network [74]. The signal at 869 cm^{-1} is attributed to a Si-O terminal bond of a typical N-A-S-H gel, as reported

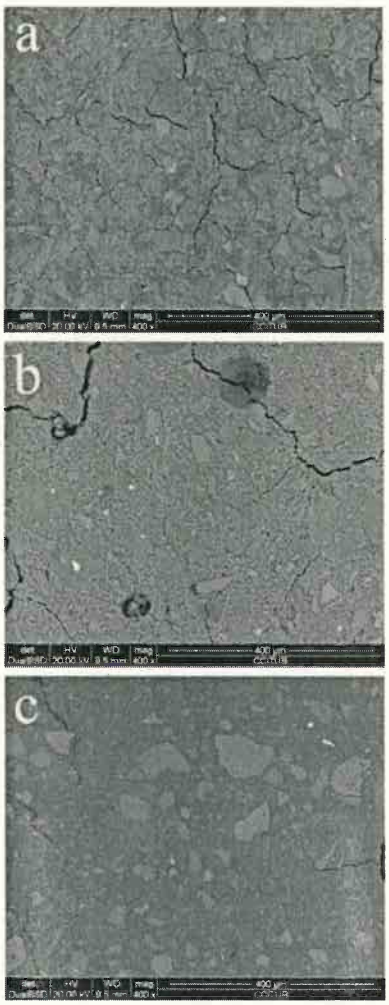

Fig. 8. SEM micrographs of AA-WBA/MK binders (a) 100 W (b) 50W50M (c) 100 M.

elsewhere [75]. These results agree with the XRD analysis, which demonstrated the presence of secondary reaction products of the N-A-S-H gel. However, in samples with high WBA-content (75W25M and 100 W), the shift to lower frequencies was less pronounced due to the formation of C-(A)-S-H gel structure, which produces displacement to higher frequencies [76]. The presence of a C-(A)-S-H gel was also verified in XRD analysis with the gehlenite and tokkoite identification. Regarding the influence of curing time, only formulations with high-WBA content (75W25M and 100 W) showed substantial changes from 60 days. The main band shifted towards higher frequencies, which revealed the carbonation of the samples [77]. This carbonation also altered the peaks ascribed to the stretching (1436 cm^{-1} and 1408 cm^{-1}) and bending modes (875 cm^{-1} and 713 cm^{-1}) of CO_3^{2-}. These peaks become wide and higher. In addition, new CO_3^{2-} peaks also appeared at 1452 cm^{-1} and 1394 cm^{-1} [78], which could be associated with the presence of natron, as observed in XRD analysis. Finally, the two signals at 796 cm^{-1} and 776 cm^{-1} also agreed with XRD results since they revealed the presence of unreacted quartz contained in WBA [79].

The FT-IR spectra of most representative samples (100 W, 50W50M and 100 M) compared to the RFs after their selective chemical extractions are shown in Fig. 7. The characteristic broadband (~1000 cm^{-1}) associated with C-(A)-S-H and N-A-S-H phases was shifted to a higher wavenumber in all the RFs, which indicated the dissolution of these gels after SAM and HCl extraction [64]. However, the position of the characteristic broadband in the RF after SAM and HCl extraction of the 100 W sample remained unaltered, which demonstrated the C-(A)-S-H nature of the gel formed in the 100 W sample. In contrast, in the 50W50M and 100 W samples, the RFs spectra varied significantly, with RF after HCl extraction being the most displaced. This revealed the (C, N)-(A)-S-H and N-A-S-H nature of the 50W50M and 100 W samples, respectively. The broadbands and peaks that remained at 790 cm^{-1}, 930 cm^{-1} and 1050 cm^{-1} after SAM (in the 100 W sample) and HCl extraction (in all samples) can be considered characteristics of silica gel [80].

Table 6
SiO_2/Al_2O_3 and Al_2O_3/Na_2O ratios of 100 M, 50W50M, and 100 M samples.

Sample	SiO_2/Al_2O_3 ratio	Na_2O/Al_2O_3 ratio
Matrix area		
100 M	1.98	0.58
50W50M	2.98	0.76
100 W	15.56	3.32
Particles area		
100 M	264.42	0.11
50W50M	32.53	4.50
100 W	34.78	4.56

3.3.2.3. Scanning electron microscopy (SEM) analysis. The SEM images in the backscattering electron (BSE) mode of the most representative samples (100 W, 50W50M and 100 M) are shown in Fig. 8. Although the formation of a cement-based compact matrix and a large number of unreacted particles was seen in all samples, the microstructure substantially varied depending on the content of WBA and MK. The presence of more microcracks in the 100 W sample is probably due to their higher volume shrinkage compared with 50W50M and 100 M samples. The percentage of volume shrinkage in the 100 W sample was 21%, while in the 50W50M and 100 M samples were 0.1% and 3%, respectively. Consequently, the higher the drying shrinkage, the higher formation of microcracks, as demonstrated in the literature [81].

The SEM-EDS analysis allowed the chemical composition of the cementitious matrix and the unreacted particles of the three samples to be determined. The average SiO_2/Al_2O_3 and Na_2O/Al_2O_3 ratios (20 measures per sample area) are summarized in Table 6. In all cases, lower ratios were determined in the matrix area than expected theoretically (Table 1). The lower value of the Na_2O/Al_2O_3 ratio was because of the migration of the Na element under the electron beam [82]. The lower SiO_2/Al_2O_3 ratio was probably due to the lower reaction of SiO_2 than expected by the chemical attack with NaOH 8 M. The chemical attacks were carried out with an excess of NaOH, so the pH of the solution was higher than commonly used as an alkaline activator. A downward trend was also observed in the SiO_2/Al_2O_3 and Na_2O/Al_2O_3 ratios as the MK content increased, due to the higher reactive Al_2O_3 availability. A lack of aluminium was evidenced in the 100 W sample because of the effective non-ferrous metal recovery treatment of IBA in particles above 8 mm [11]. The SiO_2/Al_2O_3 and Al_2O_3/Na_2O average ratios in the 100 W and 50W50M formulations revealed the glass nature of the particles due to the primary and secondary glass contained in the coarse polluted fraction of WBA [11,53]. The average ratios obtained in the 100 M sample demonstrated that the unreacted particles are silicon phases such as quartz.

3.3.3. Physical and mechanical characterisation

Fig. 9 depicts the bulk density, porosity, and compressive strength of each AA-WBA/MK binders' formulation at 28 days of curing. An increase in porosity was noticed as the amount of MK increased. This was probably due to the increase of the L/S ratio (see Table 1), which leads to an increase in initial water content. The dominant factor influencing porosity and density in metakaolin-based geopolymers is the "free water" [83]. This "free water" evaporates as specimens are cured, which leaves porosity in the matrix microstructure. The high density of the 100 W sample compared to other studies [32,72] was due to the use of 8 to 30 mm, whose amount of metallic aluminium is low compared to fine

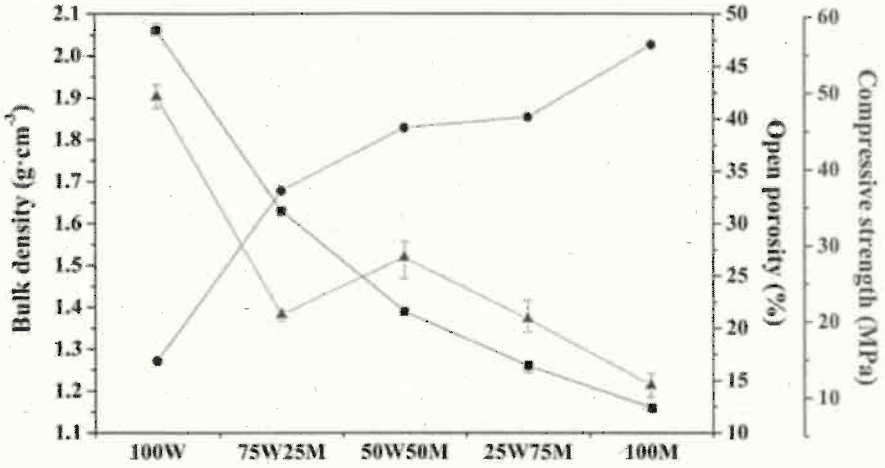

Fig. 9. Bulk density and porosity of AA-WBA/MK binders at 28 days of curing.

Table 7
Mercury intrusion porosimetry (MIP) results.

Sample	Pore volume ($mL \cdot g^{-1}$)	Pore area (m^2/g)	Average pore diameter (μm)	Porosity (%)	Bulk density ($g \cdot cm^{-3}$)
100 W	0.089	4.392	0.0812	16.87	2.06
75W25M	0.231	22.735	0.0406	33.13	1.63
50W50M	0.333	41.312	0.0266	39.12	1.39
25W75M	0.377	45.031	0.0334	40.17	1.26
100 M	0.405	37.129	0.0436	47.07	1.22

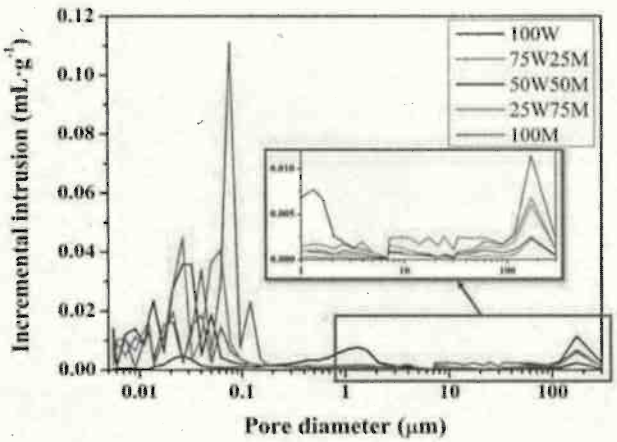

Fig. 10. Incremental intrusion curve of AA-WBA/MK binders at 28 days of curing.

fractions [13]. A downward trend in bulk density and compressive strength was also observed as the amount of MK in formulations increased. This agrees with the porosity results (except for the 75W25M sample). In the 75W25M sample, the porous network plays an important role in decreasing its compressive strength.

Table 7 summaries the mercury intrusion porosimetry (MIP) results obtained on the 28-day curing samples. It was demonstrated that the presence of WBA in the matrix reduced the total porosity of AA-WBA/MK binders compared with the 100 M sample. The total pore volume (corresponding to the Hg volume permeated) followed the same trend. However, the trend in the total pore area was linked to the dimension of the pores. The introduction of WBA into AA-WBA/MK binders led to an

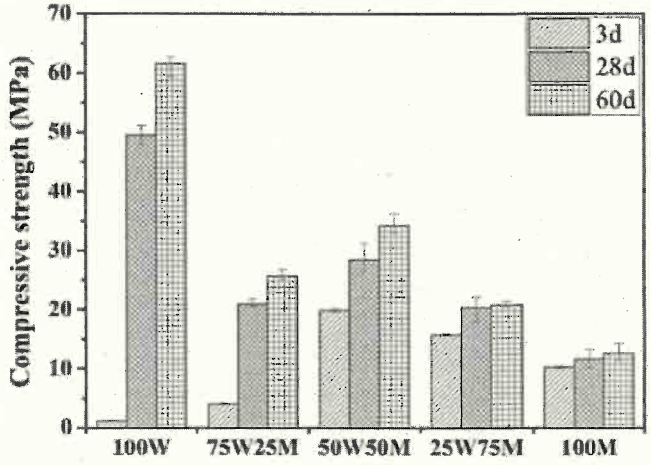

Fig. 11. Compressive strength of AA-WBA/MK binders at 3, 28, and 60 days.

increase in the total pore area until 50 wt% of WBA. Higher amounts of WBA in the binder matrix also led to a decrease in the composition prepared with WBA (9 times lower in the 100 M sample). Simultaneously, the size of the pores decreased (up to 50% WBA) and then increased and reached the lowest value in the sample 50W50M.

The incremental intrusion curve vs. pore diameter (Fig. 10) revealed the pore size distribution for AA-WBA/MK binders. The curve of the 75W25M sample revealed that its pore size distribution was higher than the rest (see the enlarged image of Fig. 10), which reinforces the coherence in the results obtained for porosity. These larger pores contributed to a reduction in the strength of binders [84]. The 50W50M sample had a lower pore size distribution than the 100 M sample. The main peak for the 100 M sample (0.103 μm) was displaced to (0.046 μm) for the 50W50M sample. The pore size distribution of the 100 W sample was very different, with large capillary pores concentrated around 173, 1.33 and small pores at 0.026 μm. This distribution demonstrates that the microstructure of the 100 W sample was different from that of the rest of the formulations.

Fig. 11 depicts the compressive strength of AA-WBA/MK binders at different ages (3, 28 and 60 days). A general downward trend was observed as the MK content increased. The sample 75W25M did not follow this trend, probably because of the lower amount of alkaline activator used. However, this amount was used because of the authors' interest in adjusting the Na_2O/Al_2O_3 ratio of formulations containing MK to favour the dissolution step of Si^{4+} and Al^{3+} and enhance the

Table 8
Leaching concentrations (mg·kg^{-1}) on AA-WBA/MK binders after leaching test (EN 12457–2) and limits for acceptance at landfills.

	As	Ba	Cd	Cr	Cu	Hg	Mo	Ni	Pb	Sb	Se	Zn
28 days												
100 W	2.25	0.69	<0.01	0.62	0.79	<0.01	0.33	0.10	0.78	5.58	0.12	0.19
75W25M	4.17	0.12	<0.01	0.36	0.64	<0.01	0.29	0.07	0.13	2.40	0.19	0.01
50W50M	4.01	0.05	<0.01	0.13	0.30	<0.01	0.26	0.05	0.03	0.46	0.25	0.01
25W75M	5.30	0.03	<0.01	0.43	0.28	<0.01	0.23	0.03	0.02	0.20	0.27	0.01
100 M	7.21	0.03	<0.01	0.61	0.25	<0.01	0.20	0.03	0.04	0.03	0.27	0.01
60 days												
100 W	2.21	0.46	<0.01	0.35	0.60	<0.01	0.43	0.08	0.42	3.54	0.20	0.11
75W25M	4.10	0.09	<0.01	0.26	0.37	<0.01	0.33	0.04	0.06	0.95	0.20	<0.01
50W50M	2.34	0.03	<0.01	0.09	0.23	<0.01	0.23	0.02	0.01	0.30	0.20	<0.01
25W75M	3.77	0.04	<0.01	0.43	0.20	<0.01	0.21	0.03	0.02	0.11	0.20	<0.01
100 M	4.18	0.02	<0.01	0.45	0.14	<0.01	0.15	0.02	0.01	0.02	0.20	<0.01
[1]Inert waste (mg·kg^{-1})	0.5	20	0.04	0.5	2	0.01	0.5	0.4	0.5	0.06	0.1	4
[1]Non-hazardous waste (mg·kg^{-1})	2	100	1	10	50	0.2	10	10	10	0.7	0.5	50
[1]Hazardous waste (mg·kg^{-1})	25	300	5	70	100	2	30	40	50	5	7	200

[1] limit for acceptance at landfills[57]

polymerization process, as reported in the literature [62]. Another hypothesis is that the low pH value of the alkaline activator in the formulation of 75W25M sample (12.9) hinders the dissolution of the aluminosilicate phases of MK. The authors demonstrated that lower pH (pH < 13) was required for the alkaline activation of the WBA in other studies [54,55]. However, the 75W25M sample may have required a higher pH value similar to a NaOH 8 M solution as it contained a high content of aluminosilicate phases from MK [85]. An upward trend was observed as the curing time of the samples increased. This trend was more pronounced in samples that contained up to 50% of WBA. The increase in strength was especially significant in the 100 M formulation, where it was multiplied by 50.

The highest compressive strength was obtained in the 100 W sample (61.6 MPa), while the lowest was found in the 100 M sample (12.6 MPa). The results evidenced the possibility of obtaining AA-WBA/MK with good mechanical performance comparable to OPC pastes [86,87], depending on the content of WBA and MK. Moreover, the mechanical properties improved significantly compared to other studies that use WBA as the sole precursor [88] or as partial precursor mixed with MK [42]. Note that the use of 25 mm cubic specimens influences the compressive strength values. Indeed, a conversion coefficient (0.7–0.86) needs to be applied to compare them with 40 mm cubic standardised specimens [89].

3.3.4. Environmental characterisation

The leaching potential of the AA-WBA/MK binders was assessed through the EN 12457–2 and the CEN/TS 16637–2 standards. The former was used to simulate the leaching potential of the binders at the end of life. The leaching concentration of 12-heavy metal(loid)s after 28 and 60 days of curing was evaluated by means of a leaching test in deionised water (liquid to solid ratio = 1/10 L·kg^{-1}) for 24 h. The leaching concentration of heavy metal(loid)s and the leaching limit values for its acceptance at landfills are summarised in Table 8. The results obtained at 28 days showed that the concentration of As, Cr, Cu, Mo, Sb and Se increased in terms of the leaching values of raw materials (Table 3). However, seven metals (Ba, Cd, Cu, Hg, Mo, Ni and Zn) were found to be below the acceptance limits for inert waste at landfills. Another three metals (Cr, Pb, and Se) could be classified as inert or non-hazardous waste depending on the formulation. The main drawback was observed for the values of As and Sb (except the 100 M sample), which exceeded the limit values for non-hazardous waste. This means that As and Sb were activated by the alkaline activator solution due to its high alkalinity [31]. The high pH environment contributed to the anionic species of these pH-dependent metalloids, as reported elsewhere [90]. As and Sb are found in WBA in oxide form because they are used in the glass industry to remove bubbles and as colouring agents [55]. As for MK, As is commonly adsorbed from kaolinite and easily desorbed in high-pH environments [91]. However, the results at 60 days showed a significant downward trend in heavy metal(loid) leaching concentrations, except for the As in the 100 W and 75W25M samples. Therefore, it was demonstrated that the encapsulating effect improves with curing time. This is consistent with another study, which revealed that the encapsulation efficiency increases after long curing periods [92].

The CEN/TS 16637–2 standard was conducted to reproduce the leaching potential during the service life of AA-WBA/MK binders. Table 9 shows the leaching concentrations and the restriction limits for its use as a construction material, established in Dutch standard (NEN 7345). Materials with leaching values below the U_1 limit do not have any environmental restrictions on their use; the choice will only depend on physical and structural criteria. There are no restrictions on the use of materials with leaching concentrations between U_1 and U_2 but it is mandatory to extract the pollutant at the end of the life of this material. Finally, materials with leaching values exceeding the U_2 limit have restricted use. Taking into account the regulatory considerations, 50W50M, 25W75M and 100 M samples could be used as construction materials without any restrictions. However, at some leaching concentration values (As, Sb, Se and V), the heavy metal(loid)s that exceeded the U_1 limit should be extracted. In the 100 W and 75W25M samples, the leaching concentration of Sb exceeded the U_2 value, which limits their use. Note the high leaching concentrations of As (in all samples), Sb (100 W and 75W25M samples), and V (samples activated with MK). The presence of As and Sb was described above, while the presence of V is

Table 9
Leaching concentrations (mg·m^{-2}) on AA-WBA/MK binders after tank leaching test (CEN/TS 16637–2) and restriction limits for its use as construction material.

Sample	As	Ba	Cd	Cr	Cu	Hg	Mo	Pb	Ni	Sb	Se	Sn	V	Zn
100 W	33.1	13.5	1.6	19.9	19.4	0.1	4.1	1.9	20.1	56.4	1.8	3.4	8.7	27.5
75W25M	57.6	1.9	0.6	9.2	10.1	0.1	3.9	1.9	3.6	27.7	3.0	0.4	236.4	11.1
50W50M	37.7	0.8	0.2	5.1	5.6	0.0	2.2	0.6	0.4	15.8	2.6	0.2	262.9	20.7
25W75M	41.7	0.6	0.0	2.5	5.0	0.0	1.9	0.5	0.3	4.4	2.8	0.3	340.9	2.9
100 M	53.7	0.6	0.1	2.9	4.1	0.0	1.6	0.4	0.4	0.8	3.4	0.3	450.4	4.4
U_1(mg·m^{-2})	40	600	1	150	50	0.4	15	100	50	3.5	1.5	25	250	200
U_2(mg·m^{-2})	300	4500	7.5	950	350	3	95	800	350	25	9.5	200	1500	1500

due to the retention of this element by kaolin, as reported elsewhere [93].

4. Conclusions

Valorisation of municipal solid waste incineration bottom ash is one of the main challenges in waste management, due to the large amount produced worldwide. This research showed the potential of WBA as an alkali-activated precursor (alone or mixed with MK) to obtain medium–high strength binders to be applied in civil and building engineering. The synergistic combination of WBA and MK reduces the leachate metal(loid) toxicity of AA-WBA/MK binders.

The microstructure of AA-WBA/MK binders revealed the formation of typical secondary products from alkali activation of MK and WBA. As expected, crystalline phases from N-A-S-H gel were only observed in the 100 M sample, due to the low calcium composition of MK. In the rest of the samples, a combination of crystalline phases from C-(A)-S-H, (C,N)-A-S-H and N-A-S-H gels were observed. The effect of curing time on the carbonation of the samples that contain at least 50% of WBA was also demonstrated. This is due to the remaining unreacted alkaline activator, which is carbonated and leads to the formation of sodium carbonate phases. Concerning the selective chemical extractions, an interference in SAM extraction was discovered that shows that this test may be inconsistent since it dissolves other phases apart from C-(A)-S-H gel phases.

The effect and relationship between the porous network and the compressive strength of AA-WBA/MK binders were demonstrated. The physical results also revealed a generalised upward trend in porosity as the MK content increased. This is because of unreacted water ("free water") of alkaline activator solution in the increase in porosity. Only the 75W25M sample breaks this trend since it has the largest pore size.

The environmental characterisation demonstrated the effect of increasing curing time on the decreasing leaching metal(loid) concentration of AA-WBA/MK binders. However, the leaching potential of As and Sb should be further investigated to assure their stabilisation in longer curing periods. It was observed that the addition of 50% of MK enhanced the encapsulation effect of AA-WBA/MK binders, so that they could be used without any environmental restrictions, according to Dutch regulation NEN 7345.

Declaration of Competing Interest

The authors declare that they have no known competing financial interests or personal relationships that could have appeared to influence the work reported in this paper.

Acknowledgements

The work is partially funded by the Spanish Government (BIA2017-83912-C2-1-R). The authors would like to thank the Catalan Government for the quality accreditation given to their research group DIOPMA (2017 SGR 118). We also want to thank SIRUSA and VECSA for supplying MWI Bottom Ash. Mr. Alex Maldonado-Alameda is grateful to the Government of Catalonia for the research Grant (FI-DGR 2017). Dr. Jessica Giro-Paloma is a Serra Húnter Fellow.

References

[1] Publ. Off. Eur. Union. (2010) 20, https://doi.org/10.2779/93548.
[2] E. Commision, An EU action plan for the circular economy 614 (2015) 21, https://doi.org/10.1017/CBO9781107415324.004.
[3] European Commission, Towards a circular economy – Waste management in the EU, 2017. https://doi.org/10.2861/978568.
[4] T.W. Assmuth, T. Strandberg, Ground water contamination at Finnish landfills, Water. Air. Soil Pollut. 69 (1-2) (1993) 179–199.
[5] X.F. Lou, J. Nair, Bioresource Technology The impact of landfilling and composting on greenhouse gas emissions – A review, Bioresour. Technol. 100 (16) (2009) 3792–3798, https://doi.org/10.1016/j.biortech.2008.12.006.
[6] A. Kasassi, P. Rakimbei, A. Karagiannidis, A. Zabaniotou, Bioresource Technology Soil contamination by heavy metals : Measurements from a closed unlined landfill 99 (2008) 8578–8584, https://doi.org/10.1016/j.biortech.2008.04.010.
[7] M. Ahel, N. Mikac, B. Cosovic, E. Prohic, V. Soukup, The impact of contamination from a municipal solid waste landfill (Zagreb, Croatia) on underlying soil, Water Sci. Technol. 37 (1998) 203–210.
[8] European Commission, Municipal waste by waste management operations, Eurostat. (2019). https://appsso.eurostat.ec.europa.eu/nui/show.do?dataset=env_wasmun&lang=en (accessed May 4, 2021).
[9] Brussels (2017). http://ec.europa.eu/priorities/energy-union-and-climate/state-energy-union_en%0Ahttps://ec.europa.eu/environment/waste/waste-to-energy.pdf.
[10] H. Cheng, Y. Hu, Municipal solid waste (MSW) as a renewable source of energy: Current and future practices in China, Bioresour. Technol. 101 (11) (2010) 3816–3824, https://doi.org/10.1016/j.biortech.2010.01.040.
[11] R. del Valle-Zermeño, J. Gómez-Manrique, J. Giro-Paloma, J. Formosa, J. M. Chimenos, Material characterization of the MSWI bottom ash as a function of particle size. Effects of glass recycling over time, Sci. Total Environ. 581-582 (2017) 897–905, https://doi.org/10.1016/j.scitotenv.2017.01.047.
[12] D. Blasenbauer, F. Huber, J. Lederer, M.J. Quina, D. Blanc-Biscarat, A. Bogush, E. Bontempi, J. Blondeau, J.M. Chimenos, H. Dahlbo, J. Fagerqvist, J. Giro-Paloma, O. Hjelmar, J. Hyks, J. Keaney, M. Lupsea-Toader, C.J. O'Caollai, K. Orupõld, T. Pajak, F.-G. Simon, L. Svecova, M. Šye, R. Ulvang, K. Vaajasaari, J. Van Caneghem, A. van Zomeren, S. Vasarevičius, K. Wégner, J. Fellner, Legal situation and current practice of waste incineration bottom ash utilisation in Europe, Waste Manag. 102 (2020) 868–883, https://doi.org/10.1016/j.wasman.2019.11.031.
[13] S. Pérez-Martínez, J. Giro-Paloma, A. Maldonado-Alameda, J. Formosa, I. Queralt, J.M. Chimenos, Characterisation and partition of valuable metals from WEEE in weathered municipal solid waste incineration bottom ash, with a view to recovering, J. Clean. Prod. 218 (2019) 61–68, https://doi.org/10.1016/j.jclepro.2019.01.313.
[14] J.M. Chimenos, A.I. Fernández, R. Nadal, F. Espiell, Short term natural weathering of MSWI bottom ash, J. Hazard. Mater. B79 (79) (2000) 287–299, https://doi.org/10.1016/S0304-3894(00)00270-3.
[15] O. Hjelmar, J. Holm, K. Crillesen, Utilisation of MSWI bottom ash as sub-base in road construction: First results from a large-scale test site, J. Hazard. Mater. 139 (3) (2007) 471–480, https://doi.org/10.1016/j.jhazmat.2006.02.059.
[16] E. Toraldo, S. Saponaro, A. Careghini, E. Mariani, Use of stabilized bottom ash for bound layers of road pavements, J. Environ. Manage. 121 (2013) 117–123, https://doi.org/10.1016/j.jenvman.2013.02.037.
[17] J. Pera, L. Coutaz, J. Ambroise, M. Chababbet, Use of incinerator bottom ash in concrete, Cem. Concr. Res. 27 (1) (1997) 1–5, https://doi.org/10.1016/S0008-8846(96)00193-7.
[18] J. Giro-paloma, J. Formosa, J.M. Chimenos, Granular Material Development Applied in an Experimental Section for Civil Engineering Purposes, Appl. Sci. 10 (2020) 1–15. https://doi.org/10.3390/app10196782.
[19] R. Taurino, E. Karamanova, L. Barbieri, S. Atanasova-Vladimirova, F. Andreola, A. Karamanov, New fired bricks based on municipal solid waste incinerator bottom ash, Waste Manag. Res. J. a Sustain. Circ. Econ. 35 (10) (2017) 1055–1063, https://doi.org/10.1177/0734242X17721343.
[20] Y.-S. Shim, Y.-K. Kim, S.-H. Kong, S.-W. Rhee, W.-K. Lee, The adsorption characteristics of heavy metals by various particle sizes of MSWI bottom ash, Waste Manag. 23 (9) (2003) 851–857, https://doi.org/10.1016/S0956-053X(02)00163-0.
[21] R.V. Silva, J. de Brito, C.J. Lynn, R.K. Dhir, Use of municipal solid waste incineration bottom ashes in alkali-activated materials, ceramics and granular applications: A review, Waste Manag. 68 (2017) 207–220, https://doi.org/10.1016/j.wasman.2017.06.043.
[22] B. Verbinnen, P. Billen, J.o. Van Caneghem, C. Vandecasteele, Recycling of MSWI Bottom Ash: A Review of Chemical Barriers, Engineering Applications and Treatment Technologies, Waste and Biomass Valorization. 8 (5) (2017) 1453–1466, https://doi.org/10.1007/s12649-016-9704-0.
[23] D. Xuan, P. Tang, C.S. Poon, Limitations and quality upgrading techniques for utilization of MSW incineration bottom ash in engineering applications – A review, Constr. Build. Mater. 190 (2018) 1091–1102, https://doi.org/10.1016/j.conbuildmat.2018.09.174.
[24] C. Shi, A.F. Jiménez, A. Palomo, New cements for the 21st century: The pursuit of an alternative to Portland cement, Cem. Concr. Res. 41 (7) (2011) 750–763, https://doi.org/10.1016/j.cemconres.2011.03.016.
[25] B.C. McLellan, R.P. Williams, J. Lay, A. van Riessen, G.D. Corder, Costs and carbon emissions for geopolymer pastes in comparison to ordinary portland cement, J. Clean. Prod. 19 (9-10) (2011) 1080–1090, https://doi.org/10.1016/j.jclepro.2011.02.010.
[26] I.A. Chen, Synthesis of Portland Cement and Calcium Sulfoaluminate-Belite Cement for Sustainable Development and Performance, University of Texas at Austin, 2009.
[27] M.H. Samarakoon, P.G. Ranjith, T.D. Rathnaweera, M.S.A. Perera, Recent advances in alkaline cement binders: A review, J. Clean. Prod. 227 (2019) 70–87, https://doi.org/10.1016/j.jclepro.2019.04.103.
[28] K.A. Komnitsas, Potential of geopolymer technology towards green buildings and sustainable cities, Procedia Eng. 21 (2011) 1023–1032, https://doi.org/10.1016/j.proeng.2011.11.2108.
[29] N. Roussat, J. Méhu, M. Abdelghafour, P. Brula, Leaching behaviour of hazardous demolition waste, Waste Manag. 28 (2008) 2032–2040. https://doi.org/10.1016/j.wasman.2007.10.019.

[30] S.A. Bernal, E.D. Rodríguez, A.P. Kirchheim, J.L. Provis, Management and valorisation of wastes through use in producing alkali-activated cement materials, J. Chem. Technol. Biotechnol. 91 (9) (2016) 2365–2388, https://doi.org/10.1002/jctb.4927.
[31] A. Maldonado-Alameda, J. Giro-Paloma, A. Rodríguez-Romero, J. Serret, A. Menargues, A. Andrés, J.M. Chimenos, Environmental potential assessment of MSWI bottom ash-based alkali-activated binders, J. Hazard. Mater. 416 (2021) 125828, https://doi.org/10.1016/j.jhazmat.2021.125828.
[32] Z. Chen, Y. Liu, W. Zhu, E.H. Yang, Incinerator bottom ash (IBA) aerated geopolymer, Constr. Build. Mater. 112 (2016) 1025–1031, https://doi.org/10.1016/j.conbuildmat.2016.02.164.
[33] A. Polettini, R. Pomi, E. Fortuna, Chemical activation in view of MSWI bottom ash recycling in cement-based systems, J. Hazard. Mater. 162 (2-3) (2009) 1292–1299, https://doi.org/10.1016/j.jhazmat.2008.06.018.
[34] X.C. Qiao, C.R. Cheeseman, C.S. Poon, Influences of chemical activators on incinerator bottom ash, Waste Manag. 29 (2) (2009) 544–549, https://doi.org/10.1016/j.wasman.2008.06.026.
[35] A. Wongsa, K. Boonserm, C. Waisurasingha, V. Sata, P. Chindaprasirt, Use of municipal solid waste incinerator (MSWI) bottom ash in high calcium fly ash geopolymer matrix, J. Clean. Prod. 148 (2017) 49–59, https://doi.org/10.1016/j.jclepro.2017.01.147.
[36] G. Huang, Y. Ji, L. Zhang, J. Li, Z. Hou, The influence of curing methods on the strength of MSWI bottom ash-based alkali-activated mortars: The role of leaching of OH and free alkali, Constr. Build. Mater. 186 (2018) 978–985, https://doi.org/10.1016/j.conbuildmat.2018.07.224.
[37] G. Huang, K.e. Yang, Y. Sun, Z. Lu, X. Zhang, L. Zuo, Y. Feng, R. Qian, Y. Qi, Y. Ji, Z. Xu, Influence of NaOH content on the alkali conversion mechanism in MSWI bottom ash alkali-activated mortars, Constr. Build. Mater. 248 (2020) 118582, https://doi.org/10.1016/j.conbuildmat.2020.118582.
[38] R. Onori, J. Will, A. Hoppe, A. Polettini, R. Pomi, A.R. Boccaccini, Bottom ash-based geopolymer materials: Mechanical and environmental properties, Ceram. Eng. Sci. Proc. 32 (2011) 71–82, https://doi.org/10.1002/9781118095393.ch7.
[39] I. Lancellotti, C. Ponzoni, L. Barbieri, C. Leonelli, Alkali activation processes for incinerator residues management, Waste Manag. 33 (8) (2013) 1740–1749, https://doi.org/10.1016/j.wasman.2013.04.013.
[40] I. Lancellotti, C. Ponzoni, M.C. Bignozzi, L. Barbieri, C. Leonelli, Incinerator bottom ash and ladle slag for geopolymers preparation, Waste and Biomass Valorization. 5 (3) (2014) 393–401, https://doi.org/10.1007/s12649-014-9299-2.
[41] W. Zhu, X. Hong, Y. Liu, E. Yang, Lightweight aerated metakaolin-based geopolymer incorporating municipal solid waste incineration bottom ash as gas-forming agent, J. Clean. Prod. 177 (2018) 775–781, https://doi.org/10.1016/j.jclepro.2017.12.267.
[42] B.K. Biswal, W. Zhu, E.-H. Yang, Investigation on Pseudomonas aeruginosa PAO1-driven bioleaching behavior of heavy metals in a novel geopolymer synthesized from municipal solid waste incineration bottom ash, Constr. Build. Mater. 241 (2020) 118005, https://doi.org/10.1016/j.conbuildmat.2020.118005.
[43] G. Huang, Y. Ji, J. Li, Z. Hou, C. Jin, Use of slaked lime and Portland cement to improve the resistance of MSWI bottom ash-GBFS geopolymer concrete against carbonation, Constr. Build. Mater. 166 (2018) 290–300, https://doi.org/10.1016/j.conbuildmat.2018.01.089.
[44] Y. Song, B. Li, E.H. Yang, Y. Liu, T. Ding, Feasibility study on utilization of municipal solid waste incineration bottom ash as aerating agent for the production of autoclaved aerated concrete, Cem. Concr. Compos. 56 (2015) 51–58, https://doi.org/10.1016/j.cemconcomp.2014.11.006.
[45] X. Gao, B. Yuan, Q.L. Yu, H.J.H. Brouwers, Characterization and application of municipal solid waste incineration (MSWI) bottom ash and waste granite powder in alkali activated slag, J. Clean. Prod. 164 (2017) 410–419, https://doi.org/10.1016/j.jclepro.2017.06.218.
[46] I. García-Lodeiro, V. Carcelen-Taboada, A. Fernández-Jiménez, A. Palomo, Manufacture of hybrid cements with fly ash and bottom ash from a municipal solid waste incinerator, Constr. Build. Mater. 105 (2016) 218–226, https://doi.org/10.1016/j.conbuildmat.2015.12.079.
[47] N. Cristelo, L. Segadães, J. Coelho, B. Chaves, N.R. Sousa, M. de Lurdes Lopes, Recycling municipal solid waste incineration slag and fly ash as precursors in low-range alkaline cements, Waste Manag. 104 (2020) 60–73, https://doi.org/10.1016/j.wasman.2020.01.013.
[48] Z. Ji, Y. Pei, Geopolymers produced from drinking water treatment residue and bottom ash for the immobilization of heavy metals, Chemosphere. 225 (2019) 579–587, https://doi.org/10.1016/j.chemosphere.2019.03.056.
[49] R. Kurda, R.V. Silva, J. de Brito, Incorporation of alkali-activated municipal solid waste incinerator bottom ash in mortar and concrete: A critical review, Materials (Basel). 13 (2020) 1–24, https://doi.org/10.3390/ma13153428.
[50] J. Giro-Paloma, A. Maldonado-Alameda, J. Formosa, L. Barbieri, J.M. Chimenos, I. Lancellotti, Geopolymers based on the valorization of Municipal Solid Waste Incineration residues, IOP Conf. Ser. Mater. Sci. Eng. 251 (2017) 012125, https://doi.org/10.1088/1757-899X/251/1/012125.
[51] K. Krausova, T.W. Cheng, L. Gautron, Y.S. Dai, S. Borenstajn, Heat Treatment on Fly and Bottom Ash Based Geopolymers: Effect on the Immobilization of Lead and Cadmium, Int. J. Environ. Sci. Dev. 3 (2012) 350–353.
[52] X.C. Qiao, M. Tyrer, C.S. Poon, C.R. Cheeseman, Characterization of alkali-activated thermally treated incinerator bottom ash, Waste Manag. 28 (10) (2008) 1955–1962, https://doi.org/10.1016/j.wasman.2007.09.007.
[53] A. Maldonado-Alameda, J. Giro-Paloma, A. Svobodova-Sedlackova, J. Formosa, J. M. Chimenos, Municipal solid waste incineration bottom ash as alkali-activated cement precursor depending on particle size, J. Clean. Prod. 242 (2020) 118443, https://doi.org/10.1016/j.jclepro.2019.118443.
[54] À. Maldonado-Alameda, J. Giro-Paloma, A. Alfocea-Roig, J. Formosa, J. M. Chimenos, Municipal Solid Waste Incineration Bottom Ash as Sole Precursor in the Alkali-Activated Binder Formulation, Appl. Sci. 10 (2020) 1–15, https://doi.org/10.3390/app10124129.
[55] A. Maldonado-Alameda, J. Giro-Paloma, J. Mañosa, J. Formosa, J.M. Chimenos, Alkali-activated binders based on the coarse fraction of municipal solid waste incineration bottom ash, Bol. La Soc. Esp. Ceram. y Vidr. In press (2021). https://doi.org/https://doi.org/10.1016/j.bsecv.2020.12.002.
[56] A. Maldonado-Alameda, J. Mañosa, J. Formosa, J. Giro-Paloma, J.M. Chimenos, Alkali-activated binders using bottom ash from waste-to-energy plants and aluminium recycling waste, Appl. Sci. 11 (2021) 1–15. https://doi.org/doi.org/10.3390/app11093840.
[57] Council of the European Union, Council Decision establishing criteria and procedures for the acceptance of waste at landfills pursuant to Article 16 of and Annex II to Directive 1999/31/EC, European Union, 2003.
[58] A. Gharzouni, L. Ouamara, I. Sobrados, S. Rossignol, Alkali-activated materials from different aluminosilicate sources: Effect of aluminum and calcium availability, J. Non. Cryst. Solids. 484 (2018) 14–25, https://doi.org/10.1016/j.jnoncrysol.2018.01.014.
[59] I. García-Lodeiro, N. Cherfa, F. Zibouche, A. Fernández-Jimenez, A. Palomo, The role of aluminium in alkali-activated bentonites, Mater. Struct. Constr. 48 (3) (2015) 585–597, https://doi.org/10.1617/s11527-014-0447-8.
[60] C. Ruiz-Santaquiteria, A. Fernández-Jiménez, A. Palomo, Quantitative determination of reactive SiO2 and Al2O3 in aluminosilicate materials, in: 13th Int. Congr. Chem. Cem., Madrid (Spain), 2011: pp. 1–7.
[61] Z. Tan, S.A. Bernal, J.L. Provis, Reproducible mini-slump test procedure for measuring the yield stress of cementitious pastes, Mater. Struct. Constr. 50 (2017) 1–12, https://doi.org/10.1617/s11527-017-1103-x.
[62] N. Murayama, H. Yamamoto, J. Shibata, Mechanism of zeolite synthesis from coal fly ash by alkali hydrothermal reaction, Int. J. Miner. Process. 64 (1) (2002) 1–17, https://doi.org/10.1016/S0301-7516(01)00046-1.
[63] W. Zhu, X. Chen, L.J. Struble, E.H. Yang, Quantitative characterization of aluminosilicate gels in alkali-activated incineration bottom ash through sequential chemical extractions and deconvoluted nuclear magnetic resonance spectra, Cem. Concr. Compos. 99 (2019) 175–180, https://doi.org/10.1016/j.cemconcomp.2019.03.014.
[64] S. Puligilla, P. Mondal, Co-existence of aluminosilicate and calcium silicate gel characterized through selective dissolution and FTIR spectral subtraction, Cem. Concr. Res. 70 (2015) 39–49, https://doi.org/10.1016/j.cemconres.2015.01.006.
[65] Y. Ping, R.J. Kirkpatrick, P. Brent, P.F. McMillan, C. Xiandong, Structure of Calcium Silicate Hydrate (C-S-H): Near-, Mid-, and Far-Infrared Spectroscopy, J. Am. Ceram. Soc. 82 (1999) 742–748, https://doi.org/10.1111/j.1151-2916.1999.tb01826.x.
[66] C. Gallé, Effect of drying on cement-based materials pore structure as identified by mercury intrusion porosimetry A comparative study between oven-, vacuum-, and freeze-drying, Cem. Concr. Res. 31 (2001) 1467–1477. https://doi.org/10.1016/S0008-8846(01)00594-4.
[67] C. Fernández Pereira, Y. Luna, X. Querol, D. Antenucci, J. Vale, Waste stabilization/solidification of an electric arc furnace dust using fly ash-based geopolymers, Fuel. 88 (7) (2009) 1185–1193, https://doi.org/10.1016/j.fuel.2008.01.021.
[68] J.A. Cusidó, L.V. Cremades, Environmental effects of using clay bricks produced with sewage sludge: Leachability and toxicity studies, Waste Manag. 32 (6) (2012) 1202–1208, https://doi.org/10.1016/j.wasman.2011.12.024.
[69] H.F.W. Taylor, Cement chemistry (1997), https://doi.org/10.1680/cc.25929.
[70] P.E.A. Lima, R.S. Angélica, R.F. Neves, Dissolution kinetics of Amazonian metakaolin in hydrochloric acid, Ceramica. 64 (2018) 86–90, https://doi.org/10.1590/0366-69132018643692179.
[71] M.F. Zawrah, R.A. Gado, R.M. Khattab, Optimization of slag content and properties improvement of metakaolin-slag geopolymer mixes, Open Mater. Sci. J. 12 (1) (2018) 40–57, https://doi.org/10.2174/1874088X01812010040.
[72] W. Zhu, X. Chen, L.J. Struble, E.H. Yang, Characterization of calcium-containing phases in alkali-activated municipal solid waste incineration bottom ash binder through chemical extraction and deconvoluted Fourier transform infrared spectra, J. Clean. Prod. 192 (2018) 782–789, https://doi.org/10.1016/j.jclepro.2018.05.049.
[73] I. García-Lodeiro, A. Palomo, A. Fernández-Jiménez, D.E. Macphee, Compatibility studies between N-A-S-H and C-A-S-H gels. Study in the ternary diagram Na_2O-CaO-Al_2O_3-SiO_2-H_2O, Cem. Concr. Res. 41 (9) (2011) 923–931, https://doi.org/10.1016/j.cemconres.2011.05.006.
[74] M.L. Granizo, S. Alonso, M.T. Blanco-Varela, A. Palomo, Alkaline activation of metakaolin: Effect of calcium hydroxide in the products of reaction, J. Am. Ceram. Soc. 85 (2002) 225–231, https://doi.org/10.1111/j.1151-2916.2002.tb00070.x.
[75] I. García-Lodeiro, A. Fernández-Jiménez, M.T. Blanco, A. Palomo, FTIR study of the sol-gel synthesis of cementitious gels: C-S-H and N-A-S-H, J. Sol-Gel Sci. Technol. 45 (1) (2008) 63–72, https://doi.org/10.1007/s10971-007-1643-6.
[76] F. Puertas, A. Fernández-Jiménez, M.T. Blanco-Varela, Pore solution in alkali-activated slag cement pastes. Relation to the composition and structure of calcium silicate hydrate, Cem. Concr. Res. 34 (1) (2004) 139–148, https://doi.org/10.1016/S0008-8846(03)00254-0.
[77] Z. Shi, C. Shi, S. Wan, N. Li, Z. Zhang, Effect of alkali dosage and silicate modulus on carbonation of alkali-activated slag mortars, Cem. Concr. Res. 113 (2018) 55–64, https://doi.org/10.1016/j.cemconres.2018.07.005.
[78] N. Li, N. Farzadnia, C. Shi, Microstructural changes in alkali-activated slag mortars induced by accelerated carbonation, Cem. Concr. Res. 100 (2017) 214–226, https://doi.org/10.1016/j.cemconres.2017.07.008.

[79] A. Fernández-Jiménez, A. Palomo, Mid-infrared spectroscopic studies of alkali-activated fly ash structure, Microporous Mesoporous Mater. 86 (1-3) (2005) 207–214, https://doi.org/10.1016/j.micromeso.2005.05.057.
[80] W. Zhu, X. Chen, A. Zhao, L.J. Struble, E.H. Yang, Synthesis of high strength binders from alkali activation of glass materials from municipal solid waste incineration bottom ash, J. Clean. Prod. 212 (2019) 261–269, https://doi.org/10.1016/j.jclepro.2018.11.295.
[81] R.J. Thomas, D. Lezama, S. Peethamparan, On drying shrinkage in alkali-activated concrete: Improving dimensional stability by aging or heat-curing, Cem. Concr. Res. 91 (2017) 13–23, https://doi.org/10.1016/j.cemconres.2016.10.003.
[82] B.A. Latella, D.S. Perera, D. Durce, E.G. Mehrtens, J. Davis, Mechanical properties of metakaolin-based geopolymers with molar ratios of Si/Al = 2 and Na/Al = 1, J. Mater. Sci. (2008) 2693–2699, https://doi.org/10.1007/s10853-007-2412-1.
[83] M. Lizcano, A. Gonzalez, S. Basu, K. Lozano, M. Radovic, D. Viehland, Effects of water content and chemical composition on structural properties of alkaline activated metakaolin-based geopolymers, J. Am. Ceram. Soc. 95 (7) (2012) 2169–2177, https://doi.org/10.1111/j.1551-2916.2012.05184.x.
[84] S. Jin, J. Zhou, X. Zhao, L.u. Sun, Quantitative relationship between pore size distribution and compressive strength of cementitious materials, Constr. Build. Mater. 273 (2021) 121727, https://doi.org/10.1016/j.conbuildmat.2020.121727.
[85] M. Torres-Carrasco, F. Puertas, Alkaline activation of different aluminosilicates as an alternative to Portland cement: alkali activated cements or geopolymers, Rev. Ing. Constr. 32 (2017) 5–12, https://doi.org/10.4067/s0718-50732017000200001.
[86] Y.-X. Li, Y.-M. Chen, J.-X. Wei, X.-Y. He, H.-T. Zhang, W.-S. Zhang, A study on the relationship between porosity of the cement paste with mineral additives and compressive strength of mortar based on this paste, Cem. Concr. Res. 36 (9) (2006) 1740–1743, https://doi.org/10.1016/j.cemconres.2004.07.007.
[87] P. Chindaprasirt, C. Jaturapitakkul, T. Sinsiri, Effect of fly ash fineness on compressive strength and pore size of blended cement paste, Cem. Concr. Compos. 27 (4) (2005) 425–428, https://doi.org/10.1016/j.cemconcomp.2004.07.003.
[88] B. Chen, M. Brito van Zijl, A. Keulen, G. Ye, Thermal Treatment on MSWI Bottom Ash for the Utilisation in Alkali Activated Materials, KnE Eng. 2020 (2020) 25–35. https://doi.org/10.18502/keg.v5i4.6792.
[89] F.J. Alejandre, V. Flores-Alés, R. Villegas, J. García-Heras, E. Morón, Estimation of Portland cement mortar compressive strength using microcores. Influence of shape and size, Constr. Build. Mater. 55 (2014) 359–364, https://doi.org/10.1016/j.conbuildmat.2014.01.049.
[90] J. Kiventerä, H. Sreenivasan, C. Cheeseman, P. Kinnunen, M. Illikainen, Immobilization of sulfates and heavy metals in gold mine tailings by sodium silicate and hydrated lime, J. Environ. Chem. Eng. 6 (5) (2018) 6530–6536.
[91] M. Quaghebeur, A. Rate, Z. Rengel, C. Hinz, Heavy metals in the environment: Desorption kinetics of arsenate from kaolinite as influenced by pH, J. Environ. Qual. 34 (2005) 479–486, https://doi.org/10.2134/jeq2005.0479a.
[92] I. Lancellotti, M. Catauro, F. Dal, J. Kiventer, C. Leonelli, M. Illikainen, Alkali activation as new option for gold mine tailings inertization, J. Clean. Prod. 187 (2018) 76–84, https://doi.org/10.1016/j.jclepro.2018.03.182.
[93] A. Mikkonen, J. Tummavuori, Retention of vanadium (V) by three Finnish mineral soils, Eur. J. Soil Sci. 45 (3) (1994) 361–368, https://doi.org/10.1111/j.1365-2389.1994.tb00520.x.